Oxidative Etching and Its Role in Manipulating the Nucleation and Growth of Noble-Metal Nanocrystals

Yiqun Zheng,[†] Jie Zeng,[‡] Aleksey Ruditskiy,[†] Maochang Liu,[§] and Younan Xia*,[†,§]

[†]School of Chemistry and Biochemistry, Georgia Institute of Technology, Atlanta, Georgia 30332, United States

[‡]Hefei National Laboratory for Physical Sciences at the Microscale and Department of Chemical Physics, University of Science and Technology of China, Hefei, Anhui 230026, P. R. China

[§]The Wallace H. Coulter Department of Biomedical Engineering, Georgia Institute of Technology and Emory University, Atlanta, Georgia 30332, United States

ABSTRACT: Oxidative etching plays an important role in the synthesis of metal nanocrystals. This is because the zerovalent species, including atoms, clusters, and nanocrystallites, can all be oxidized back to the ionic form and thus altering the types and distributions of products formed in both the nucleation and growth steps. In the first part of this review, we discuss the critical components needed for oxidative etching, as well as methods for enabling or preventing oxidative etching in a synthesis. We then present and analyze a number of interesting experimental observations caused by oxidative etching. In the following sections, we highlight four major applications of oxidative etching in the synthesis of metal nanocrystals, with regards to experimental controls over the crystallinity, size, shape, morphology, and growth kinetics.

KEYWORDS: *oxidative etching, nanocrystal, noble metal, crystallinity, twin defect*

1. INTRODUCTION

Oxidative etching is a common phenomenon in our everyday life. Corrosion is likely the most familiar example, which is causing severe material damage and noticeable economic loss (the annual cost of corrosion worldwide is more than 3% of the world's GDP).[1] A typical case of corrosion is rust formation. When steel is in contact with both air and water for a certain period of time, rusting will begin to occur at a specific site, and then spread to cover the entire surface (Figure 1). When an electrolyte (i.e., salt from seawater) is present, the rusting process will be greatly accelerated. This is because in addition to the regular oxidation, an electrochemical process also occurs between the metal and oxygen in air. Similar to a primary cell, zerovalent iron (Fe^0) is oxidized into its ionic form (Fe^{2+}/Fe^{3+}) on the anode, releasing electrons for the reduction of oxygen on the cathode. The electrolyte serves as a salt bridge by transferring charges from the cathode region to the anode region. The iron species continue to react with oxygen or water, thus leading to the formation of rust on the steel surface. The corrosion can also take on many other forms, such as pitting, crevice etching, intergranular exchange, galvanic replacement, and dealloying, among others.

In addition to steel, oxidative etching has also been widely observed for many other inorganic materials. Notable examples include carbon-based materials (e.g., graphite, diamond, and carbon nanotube), metal, and metal oxide nanocrystals, among others.[2–6] In this review, we will narrow our discussion down to the use of oxidative etching in the synthesis of noble-metal nanocrystals. In a general synthesis, a salt precursor is reduced (or decomposed in some cases) to zerovalent atoms, followed

Figure 1. Photograph showing the corrosion or rusting of a piece of steel. Reproduced with permission from ref 83. Copyright 1996 Bushman & Associates.

by self-nucleation and growth into clusters, seeds, and then nanocrystals.[7] When the synthesis is conducted in air, together

with the presence of a proper coordination ligand for the metal ions, the zerovalent species (including atoms, clusters, and seeds) can all be possibly oxidized back to the ionic forms during both nucleation and growth.[8] As a result, the final product has to be considered as an outcome of two opposite, yet cooperative, processes: reduction and oxidation (Figure 2a).
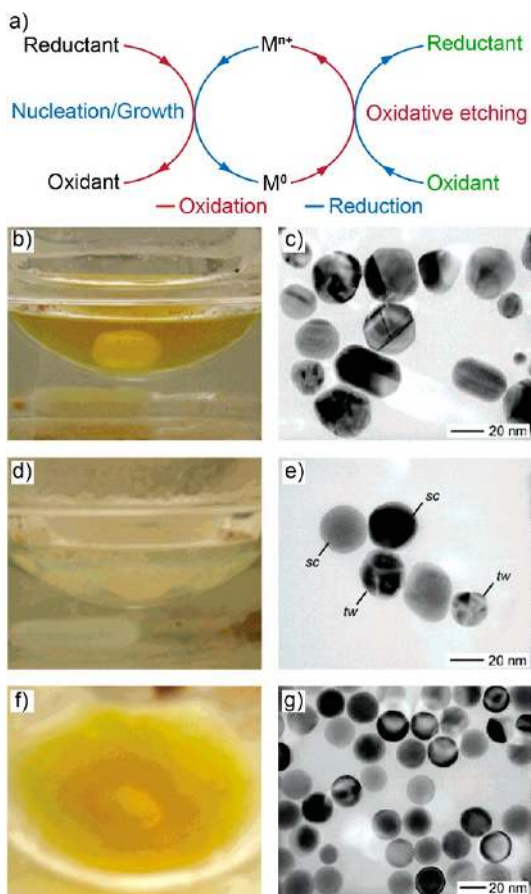

Figure 2. (a) Schematic illustration of the reduction of a metal salt precursor and oxidation of the metal that occur simultaneously in a synthesis. (b–g) Photographs and TEM images showing the changes involved in a polyol synthesis of Ag nanocrystals. Reaction times: (b, c) 10 min; (d, e) 2 h; and (f, g) 44 h. (b, d, f) Photographs of the reaction solution, in which the yellow color indicates the presence of Ag nanocrystals. (c, e, g) TEM images of the Ag nanocrystals contained in the reaction solution at the corresponding time. Single-crystal and twinned nanocrystals are labeled as *sc* and *tw*, respectively. Reproduced with permission from ref 9. Copyright 2004 American Chemical Society.

The situation becomes even more complicated when the product has twin defects on the surface, since etching tends to selectively start from the defect sites rather than a single-crystal region. This phenomenon was initially discovered during the synthesis of Ag nanocrystals, which involved the reduction of a salt precursor by a polyol.[9] The presence of Cl^- ions, combined with oxygen from air, often resulted in significant changes to the crystallinity and morphology of the final products.[10] In particular, seeds with twin defects that appeared in the early stage of a synthesis could be largely removed as reaction proceeded, and the final products were dominated by single-crystal Ag nanocrystals. This principle has enabled the synthesis of single-crystal Ag nanocubes with high quality and controlled edge length ranging from 18 to 200 nm.[11,12] Further studies

demonstrated that Ag nanocrystals with a singly twinned structure could also be produced with a yield exceeding 80% by tuning the etching strength with a different oxygen/halide pair. In addition to Ag, oxidative etching has also been observed for other noble metals, including Pd, Au, Pt, and Rh, together with the use of other types of oxidative species as etchants. To this end, we believe that oxidative etching can serve as a simple, effective, and robust method for manipulating the nucleation and growth of noble-metal nanocrystals.

In this review article, we begin with experimental observations of oxidative etching in both hydrophilic and hydrophobic systems. Several techniques have been employed to monitor this process during a synthesis in order to quantitatively understand its influence on the crystallinity and shape evolution of metal nanocrystals. We then discuss how oxidative etching could be effectively prevented to obtain nanocrystals with twinned structures. Finally, we highlight four major synthetic methods that have been enhanced or enabled by oxidative etching, including experimental controls over crystallinity, size, shape, morphology, and growth kinetics.

2. EXPERIMENTAL OBSERVATION AND MONITORING OF OXIDATIVE ETCHING

Depending on the specific metal involved, we can experimentally monitor oxidative etching using different techniques. For example, in the case of Ag, oxidative etching can be easily observed by the color change of a reaction solution due to the unique localized surface plasmon resonance (LSPR) features associated with Ag nanocrystals.[13] For instance, images b, d, and f in Figure 2 show photographs taken from the reaction solution of a polyol synthesis of Ag nanocrystals. In this case, the oxidative etching was reflected by the distinctive color changes at different stages of the synthesis.[9] Within the first few minutes of mixing, the solution became light yellow, indicating the formation of Ag nanocrystals through polyol reduction (Figure 2b). As the reaction proceeded, the yellow color started to fade away due to the dissolution of Ag nanocrystals with twinned structures, and the solution became nearly colorless at $t = 2$ h (Figure 2d). The solution remained colorless until a very light yellow color appeared again at $t = 24$ h and the color became stable after the reaction had lasted for 44 h (Figure 2f). Because the intensity of LSPR peaks is directly proportional to the concentration of Ag nanocrystals in the solution (i.e., the Beer–Lambert law), the change in color intensity offers a strong evidence to support the involvement of oxidative etching in this synthesis.

Although it is difficult to monitor a synthesis in situ because of the limitation of experimental tools, it is possible to remove aliquots of the reaction solution at different stages of a synthesis, followed by detailed characterization by transmission electron microscopy (TEM) and UV–vis extinction spectroscopy. These data can help us understand qualitatively how oxidative etching occurs as the reaction proceeds. For example, the TEM characterization of the aforementioned reaction indicated that at $t = 10$ min, most of the Ag nanocrystals were twinned (Figure 2c). By $t = 2$ h, the solution contained a mixture of twinned and single-crystal species (Figure 2e). At $t = 44$ h, the sample was free of twinned nanocrystals (Figure 2g). Corresponding UV–vis extinction spectra also confirmed this transformation process, as shown in Figure 3a. It was found that the intrinsic LSPR peak (centered at ∼400 nm) of Ag nanocrystals gradually decreased in intensity and eventually disappeared at $t = 2$ h due to the dissolution of most twinned
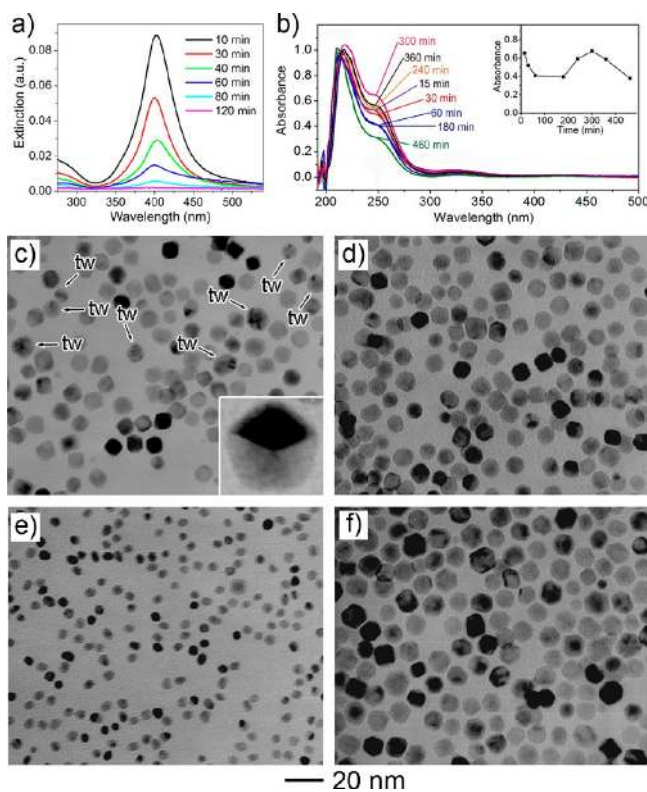
Figure 3. Monitoring the oxidative etching process using UV−vis extinction spectra. (a) UV−vis extinction spectra of six Ag samples taken from the same reaction solution between t = 10 min and t = 120 min, further confirming the disappearance of Ag nanocrystals from the solution phase during this period of synthesis. (b) UV−vis spectra of solutions taken at different reaction stages of a polyol synthesis of Pd nanocrystals. The inset depicts the time dependence of the absorbance at ~245 nm, which is directly proportional to the concentration of $[PdCl_4]^{2-}$ species. (c-f) TEM images of Pd nanocrystals obtained at (c) t = 5 min, (d) t = 180 min, (e) t = 300 min, and (f) t = 460 min. Twinned particles are indicated by *tw*. The inset of (c) shows a magnified image of a 5-fold twinned nanocrystal. (a) Reproduced with permission from ref 9. Copyright 2004 American Chemical Society. (b−f) Reproduced with permission from ref 15. Copyright 2005 American Chemical Society.

particles. This trend was in good agreement with the color change and TEM analysis illustrated in Figure 2b−g. It is believed that the defects inherent in twinned seeds of Ag led to their selective etching and dissolution by chloride and oxygen (from air), leaving only the single-crystal seeds to grow into cubes.

Alternatively, the etching process can also be tracked by monitoring the concentration of metal ions, which can be determined directly by its absorbance intensity.[14] Because reduction and oxidative etching coexist throughout the reaction, the fluctuations in concentration of metal ions indicate that the reduction and oxidative etching should alternate in dominance during the reaction period. Generally, the precursor is gradually consumed due to the reduction process in a synthesis. However, when oxidative etching starts to occur, the reduction of salt precursor will be suppressed, thus causing the concentration of precursor to increase if the rate of etching overwhelmingly exceeds that of reduction. Here, the synthesis of Pd nanocrystals is used to illustrate this concept.[15] UV−vis extinction spectra of the reaction solution were used to monitor the conversion between $[PdCl_4]^{2-}$, which has a

characteristic absorption peak at 245 nm, and elemental Pd. As shown in Figure 3b, the peak intensity decreased to its minimum after a reaction time of 60 min due to the dominance of reduction in the early stage of a synthesis. Further reaction resulted in an increase for the peak intensity, suggesting the oxidation of elemental Pd back to $[PdCl_4]^{2-}$. Ths TEM images in Figure 3, c-e, confirm the changes in particle crystallinity, size, and population. At t = 5 min (Figure 3c), the sample mainly contained cuboctahedra of 4−8 nm in size, together with 10% multiply twinned particles. A magnified image of the 5-fold twinned decahedron is shown in the inset. As the reaction proceeded to 300 min, all the twinned particles disappeared while the average size of the cubooctahedra grew to 8 nm (Figure 3d). During the next 120 min, the cuboctahedra would be slowly etched until they had reached an average diameter of 3 nm (Figure 3e). At this point, the Pd cuboctahedra began to grow again until they reached an average size of 10 nm by t = 460 min (Figure 3f). Similar to the case of Ag, the Cl^-/O_2 pair was responsible for the oxidative etching. Higher reactivity of Pd twinned particles caused them to be preferentially etched away in the early stage of a synthesis, leading to the survival of only Pd single-crystal particles in the final product.

3. OXIDATIVE ETCHING IN A HYDROPHOBIC SYSTEM

The aforementioned syntheses all involve oxidative etching during the formation of noble-metal nanocrystals in a hydrophilic solvent, such as water and ethylene glycol. Further studies indicated that oxidative etching could also occur in a hydrophobic system where hexane, toluene, chloroform, or isoamyl ether was used as the solvent. For example, we prepared Ag nanocubes in a hydrophobic system with the addition of $FeCl_3$ or $Fe(acac)_3$ as an oxidative etchant.[16] As shown in Figure 4a, if the synthesis was conducted in the absence of an oxidant (i.e., with argon protection or in the absence of Fe^{3+} species), most products took a multiply twinned structure with an icosahedral shape. In contrast, single-crystal Ag nanocubes with slight truncation at the corners were obtained when a trace amount of $FeCl_3$ was added into the system (Figure 4b). Similar to the effect of the oxygen/chloride etchant pair in a polyol system, the twinned seeds were selectively etched and oxidized back to Ag^+ ions by the Fe^{3+} species. The resultant Ag^+ ions were then reduced on the surface of existing single-crystal Ag seeds, resulting in a continuous, epitaxial growth of nanocrystals free of twin defects. The resultant Fe^{2+} species could be quickly and easily oxidized back to Fe^{3+} species by oxygen in air. The constant etching and growth, as enabled by the cycling between Fe^{3+} and Fe^{2+} species, changed the structure of Ag nanocrystals from multiply twinned into single-crystal.

The Fe-based etchant has also found use in the synthesis of ultrathin Au nanorods. The reaction was performed by aging a mixture of the $[AuCl(oleylamine)]$ complex with amorphous Fe nanoparticles in chloroform at room temperature.[17] The amorphous nature of the Fe nanoparticles which probably served as templates. These Fe nanoparticles could release to etching. At t = 12 h, Au nanoparticles with irregular shapes began to appear (Figure 4c), which exhibited a multiple-twinned structure (Figure 4d). These nanoparticles were found to be unstable in the solution, and a portion of them was found to be elongated into dumbbell-shaped nanoparticles at t = 48 h (i.e., a structure consisting of a thin rod with two enlarged ends, Figure 4e). After further aging (t = 168 h), all of the dumbbell-
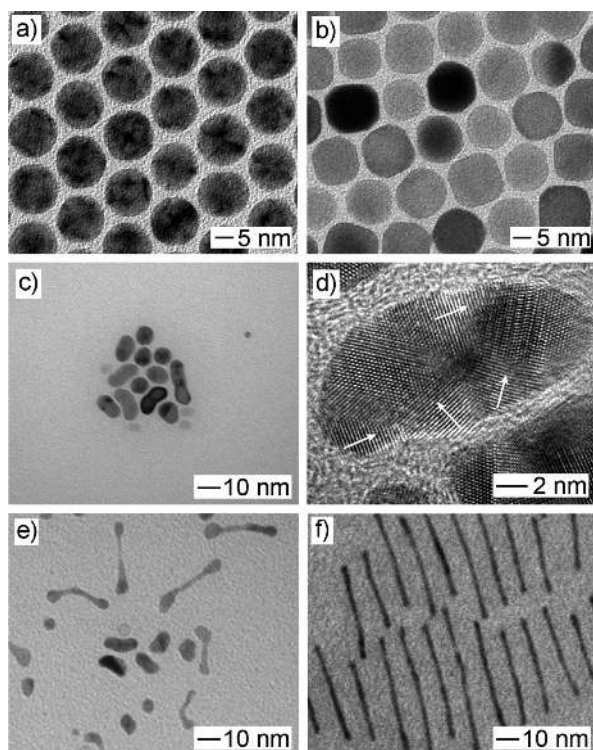
Figure 4. Examples of syntheses of noble-metal nanocrystals in hydrophobic systems involving oxidative etching. (a, b) Synthesis of small Ag nanocubes in isoamyl ether with Fe^{3+} species as an etchant. TEM images of Ag samples obtained in the (e) absence and (f) presence of Fe^{3+} species. (c–f) Synthesis of ultrathin Au nanorods in chloroform with the assistance of amorphous Fe nanocrystals. TEM images of samples obtained at different stages of a synthesis: (c) $t = 12$ h; (e) $t = 48$ h; and (f) $t = 196$ h. (d) High-resolution TEM image of a heavily defected Au nanoparticle obtained at $t = 12$ h. The arrows pointed at regions involved with twin defects. (a, b) Reproduced with permission from ref 16. Copyright 2010 Royal Society of Chemistry. (c–f) Reproduced with permission from ref 17. Copyright 2008 American Chemical Society.

shaped nanoparticles evolved into thin nanorods with a uniform diameter of ∼2 nm (Figure 4f). On the basis of these observations, it is clear that the ultrathin Au nanorods evolved from the initially formed, unstable, twinned Au nanoparticles. The defect regions of these nanoparticles would be preferentially etched and oxidized to Au^+ or Au^{3+} at a later stage of the synthesis. These Au cations were reduced again by Fe^0 or Fe^{2+} and the newly formed zerovalent Au atoms were deposited epitaxially onto the defect-free regions of the Au nanoparticles. Continuous etching and deposition eventually reshaped the nanoparticles into single-crystal nanorods, which were more stable than the original twinned particles due to reduction of defect density. In addition, recent study indicated that saturating the solution with oxygen in a similar synthesis could also lead to the production of similar products at high yields.[18] Such observations further confirm the crucial role of oxidative etching in the formation of ultrathin Au nanowires.

4. MITIGATION AND PREVENTION OF OXIDATIVE ETCHING

Despite the effectiveness of oxidative etching in the removal of twinned seeds during a synthesis, there exist situations that require the twinned nanocrystals to be the final products. In this case, oxidative etching has to be alleviated or excluded from

the reaction system. Here we provide several strategies for this purpose, along with discussions of their mechanisms.

4.1. Elimination of Oxygen. Because most of the above syntheses are conducted in air, oxygen would naturally be a part of the reaction system. To diminish the role of oxidative etching, it is essential to remove molecular oxygen from the reaction system.[19−21] For instance, Pd single-crystal nanoparticles with a cuboctahedral shape were prepared in high yields when oxidative etching was used to remove twinned particles in the early stage of the reaction.[15] In contrast, when the synthesis was conducted under argon, about 10% of the final products were found to be twinned nanocrystals. These twinned particles could be readily removed through an additional oxidative etching step by exposing the sample to air for a prolonged period of time. As a result, it is possible to exclude oxidative etching from a reaction system by conducting the synthesis under argon protection.

In addition to the use of an inert gas, oxygen molecules can also be removed from a reaction system by adding a scavenging species in the form of a redox pair. For example, a relatively high concentration of Fe^{2+} or Fe^{3+} cations, added to a synthesis of Ag nanocubes, was found to promote the formation of multiply twinned seeds, followed by the formation of penta-twinned Ag nanowires. Instead of removing twinned seeds, these Fe species removed oxygen from the surface of twinned seeds, thus preventing their dissolution by oxidative etching.[22] Similar results were obtained when Cu cations were involved.[23] As shown in Figure 5a, Ag nanowires could be obtained in large
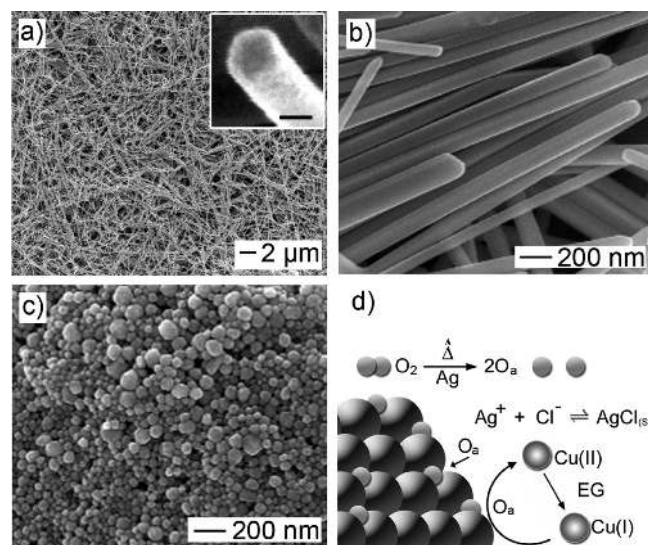

Figure 5. (a) SEM image of Ag nanowires, with the inset showing SEM image of a fractured Ag nanowire to reveal the pentagonal cross section (scale bar in the inset image: 50 nm). (b, c) SEM images from control experiments: the product obtained in the presence of (b) both CuCl and NaCl and (c) NaCl but neither Cu^{2+} nor Cu^+. (d) Schematic illustration depicting the role of Cu-containing salts in the polyol synthesis of Ag nanowires. Reproduced with permission from ref 23. Copyright 2008 Royal Society of Chemistry.

quantities in the presence of $CuCl_2$. The inset shows a pentagonal cross-section of the as-prepared nanowire, confirming its penta-twinned crystal structure. The use of Cu^+ was also found to facilitate the formation of high-quality Ag nanowires (Figure 5b), indicating that the initial oxidation state of the Cu-containing salt was irrelevant. However, when only NaCl was

added, no Ag nanowires were obtained, with only spherical Ag nanocrystals present in the final product (Figure 5c). These results indicate that Cu cations are instrumental to the formation of Ag nanowires. In particular, Cu$^+$ cations, either added directly or generated in situ from the reduction of Cu^{2+} by ethylene glycol, effectively scavenge adsorbed atomic oxygen from the Ag seeds. In this case, penta-twinned seeds were protected from being oxidized and etched away, thus facilitating the growth of Ag nanowires (Figure 5d).

4.2. Exclusion of Coordination Ligand. As discussed in the aforementioned section, a coordination ligand is necessary for oxidative etching. For example, in a typical polyol synthesis of Ag nanocubes, twinned nanoparticles with irregular shapes were obtained if no Cl$^-$ was present in the system.[11] It is possible that the ligand Cl$^-$ coordinate with Ag$^+$, pushing the equilibrium of dissolution reaction (Ag = Ag$^+$ + e$^-$) to the right side. In a sense, the exclusion of coordination ligand, halide in this case, will facilitate the protection of twinned seeds in the initial stage of the reaction, and allow for the production of twinned nanocrystals.

It is worth pointing out that the precursors for noble metals, such as Au, Pd, Pt, Rh, and Ir, usually exist as halide complexes. As a result, halide ions released from the precursors can be combined with the oxygen from air to facilitate oxidative etching during both the nucleation and growth processes.[24−29] For example, in the polyol synthesis of Rh nanocrystals, the use of Rh salt precursor with Cl$^-$, e.g., RhCl$_3$ or Na$_3$RhCl$_6$, always led to the formation of Rh nanocrystals with a single-crystal structure even if the reaction was performed under the protection of an inert gas.[30,31] This is because oxygen cannot be completely eliminated from a system and the residual oxygen molecules, even in a limited amount, can cooperate with coordination ligand to serve as an etchant. To this end, it would be advantageous to completely eliminate the etching by choosing a precursor that does not contain any halide. To this end, we demonstrated that the use of a halide-free precursor, [(CF$_3$COO)$_2$Rh]$_2$, significantly contributed to an improved yield of Rh nanocrystals with twinned defects.[32] In particular, the final product was dominated by 5-fold twinned Rh nanocrystals with five branched arms (Figure 6a). In the initial stage of the reaction, nanocrystals several nanometers in diameter were formed (Figure 6b). Analysis by high-resolution TEM imaging revealed that the sample was dominated by Rh decahedrons with tips protruding from the corners (see inset of Figure 6b). To clarify the role of halide, we systematically investigated the effect of precursor type on the crystallinity of the Rh nanocrystals. For instance, in the presence of Cl$^-$, e.g., with the use of Na$_3$RhCl$_6$ (Figure 6c) or [Rh(CF$_3$COO)$_2$]$_2$ + HCl (1:1 molar ratio, Figure 6d) as a precursor, single-crystal Rh nanocrystals in the form of tripods and other irregular shapes were obtained. Conversely, nanocrystals containing at least one twin defect were obtained when Cl-free precursors were used, such as [Rh(CH$_3$COO)$_2$]$_2$ (Figure 6e) or [Rh(CF$_3$COO)$_2$]$_2$ + citric acid (Figure 6f). On the basis of these results, it is not unreasonable to consider the exclusion of halide in the system as a critical measure to eliminate oxidative etching, allowing for the formation of Rh nanocrystals with twinned defects.

4.3. Use of an Antioxidant. It is worth pointing out that the binding of oxygen molecules to the surface of a noble-metal nanocrystal can sometimes be too strong to counteract. Therefore, if a halide is still involved in the synthesis, alternative approaches must be used to achieve efficient
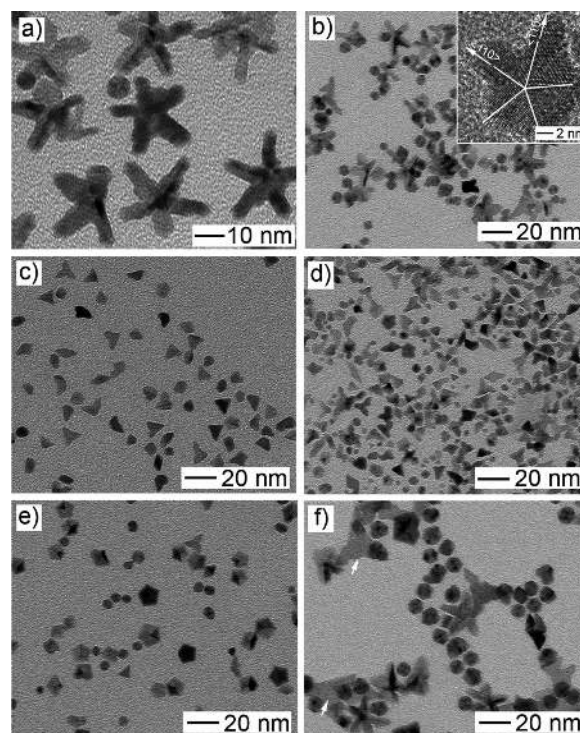

Figure 6. (a) TEM image of a typical sample of starfishlike Rh nanocrystals. (b) TEM image of Rh nanocrystals obtained 1 min after injection of precursor. The inset shows a high-resolution TEM image taken from the sample showing its penta-twinned crystal structure. (c−f) TEM images of Rh nanocrystals generated using (c) Na$_3$RhCl$_6$, (d) [Rh(CF$_3$COO)$_2$]$_2$ + HCl, (e) [Rh(CH$_3$COO)$_2$]$_2$, and (f) [Rh-(CF$_3$COO)$_2$]$_2$ + citric acid, as precursor. The white arrow in f indicated the formation of Rh nanoplates in the presence of citric acid, which should be attributed to their strong binding to the {111} facets. Reproduced with permission from ref 32. Copyright 2010 Wiley−VCH.

replacement or desorption of oxygen molecules from the surface in order to prevent oxidative etching. The introduction of an antioxidant provides a synthetic method for realizing this. In a water-based synthesis of Pd nanocrystals, the introduction of citric acid or citrate ions was found to significantly improve the yield of multitwinned particles (MTPs).[33] As shown in Figure 7, the yield of MTPs increased with the increase in concentration of citric acid added into the system. Such observation indicates that the citrate species protects the multiply twinned seeds from oxidative etching. In fact, it is well-documented that citric acid or citrate ions can strongly bind to the {111} facets of Pd (or Ag) nanocrystals and serve as capping agents to stabilize twinned Pd nanocrystals enclosed by {111} facets (i.e., decahedrons and icosahedrons), as well as single-crystal octahedrons. Owing to their strong binding to the Pd surface, these species compete with the oxygen adsorption process, thus reducing the amount of oxygen bound to the metal surface. Furthermore, citrate is a well-known antioxidant and can react with, and thus exhaust, the adsorbed oxygen. Combined together, these two effects block oxidative etching under the same reduction kinetics. Accordingly, the multiply twinned seeds were preserved, and thus accumulated, during the reaction. Similar observation was also noted in the synthesis of Pd decahedrons, where their yield was found to increase significantly by increasing the concentration of citric acid or citrate ions.[34]
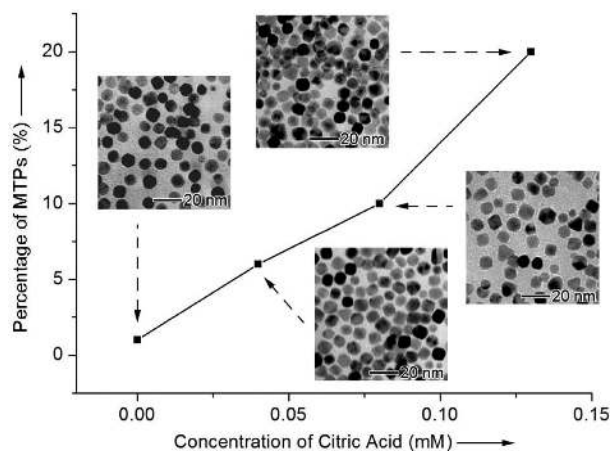
Figure 7. Correlation between the percentage of Pd MTPs and the concentration of citric acid. The number of MTPs was counted for both icosahedra and decahedra. The insets show TEM images of samples synthesized under the corresponding conditions. Reproduced with permission from ref 33. Copyright 2007 Wiley−VCH.

5. APPLICATION OF OXIDATIVE ETCHING

5.1. Control of Crystallinity. Oxidative etching has been demonstrated in several systems with the ability to manipulate the ratio of multiply twinned to single-crystal nanocrystals in the final product. This capability can be extended to manipulate the distribution of seeds with different twin structures in a more versatile way. For example, by a simply replacing Cl$^-$ with Br$^-$ in a polyol synthesis of Ag nanocrystals, the yield of singly twinned nanocrystals, with a shape of right bipyramid, increased to over 80%.[35] When the reaction was allowed to proceed for 3 and 5 h, respectively, their edge lengths increased from 75 to 150 nm (Figure 8a, b). When the reaction was stopped at 1.5 h, spherical particles with single twinned structure were found
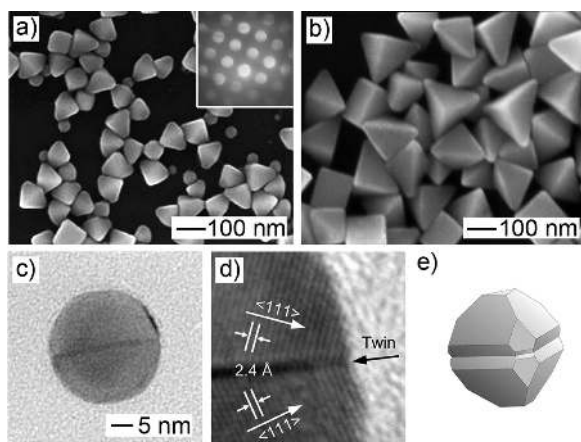
Figure 8. (a, b) SEM images of Ag right bipyramids approximately (a) 75 nm and (b) 150 nm in edge length. The inset in a shows the electron diffraction pattern obtained from a single bipyramid, indicating that it is bounded by {100} facets. (c) At t = 1.5 h, single twinned seeds approximately 25 nm in diameter were observed. (d) HRTEM of a twinned seed shows the lattice fringes reflecting across the (111) twin plane. (e) Model of the seed in C showing (111) truncation of corners, reentrant (111) surfaces at the twin boundary and reentrant (100) surfaces at the twin boundary corners. Reproduced with permission from ref 35. Copyright 2006 American Chemical Society.

(Figure 8c). The reflection of lattice fringes across the twin plane is evident in a high-resolution TEM image of the twinned seed (Figure 8d). An approximate seed structure rendered in three dimensions is shown in Figure 8e. These singly twinned seeds were necessary for the further growth of right bipyramids. Their continued existence post etching can be explained by the fact that Br$^-$ is less corrosive than Cl$^-$. The Br$^-$ ions enabled sufficient etching to eliminate the seeds with multiple twin defects, but were not adequately strong to eliminate those seeds with only one twin defect. It is worth pointing out that when the concentration of Br$^-$ was doubled, the resultant nanocrystals became rectangular bars with a single-crystal structure.[36,37] This is due to the enhancement of oxidative etching at high concentration of Br$^-$, facilitating the formation of the anisotropic structures. The slower reduction kinetics associated with AgBr might also contribute to the anisotropic growth, as we demonstrated in most recent work.[38−40] Taken together, it is possible to single out Agnanocrystals with single-crystal, singly twinned, or multiply twinned structures by using etchants with different strengths or the same etchant at different concentrations.

5.2. Control of Growth Mode. It is well-known that the nucleation and growth of a nanocrystal is highly sensitive to the rate at which the atoms are generated from a precursor.[41−43] In fact, oxidative etching can retard the reduction of a salt precursor, leading to a significant slowdown in the reaction kinetics. As a result, this allows us to manipulate the atomic deposition rate and thereby cause changes to the growth mode.[44] For example, it was found that anisotropic deposition of Ag atoms on an as-formed cubic seed could be facilitated due to the presence of oxidative etching.[45] In this case, the Ag cubes were transformed into anisotropically truncated octahedrons soon after the addition of Ag precursor (Figure 9a). Rather than being added to all six faces of the cube evenly, the Ag atoms were added to three adjacent {100} faces more rapidly than the other three {100} faces (Figure 9b). In this case, some Ag atoms were oxidized back to Ag$^+$ prior to deposition on a cubic seed, making the concentration of Ag atoms too low to allow nucleation on multiple faces of the seed. This growth mode eventually led to the formation of asymmetrically truncated octahedrons. In contrast, when the reaction was conducted under the protection of argon, oxidative etching was depressed and thus the reduction of Ag$^+$ is left uninhibited. In this case, the concentration of Ag atoms could be maintained at a level sufficiently high to facilitate nucleation on all faces of a cubic seed, leading to a conformal growth and the formation of Ag nanocubes as the final product (Figure 9c). This principle was demonstrated in a more direct way in our most recent work, which showed that selective nucleation and growth of Ag on one, three, or six of the equivalent {100} faces of a cubic Pd or Ag seed could occur depending on the kinetics. Unlike the use of oxidative etching, the concentration of Ag atoms was directly controlled by simply varying the rate at which the Ag precursor was introduced with a syringe pump and reduced to atoms.[38−40] These demonstrations clearly support the role of oxidative etching in manipulating reaction kinetics and thus control of growth mode.

5.3. Control of Size. The etching that occurs in the nucleation stage can also be used to control the particle size. When the initially formed seeds are oxidized into precursor ions, they will be subsequently reduced and deposited on the remaining seeds in the solution, thus increasing their size. Such a cycle can be repeated throughout the synthesis, increasing the
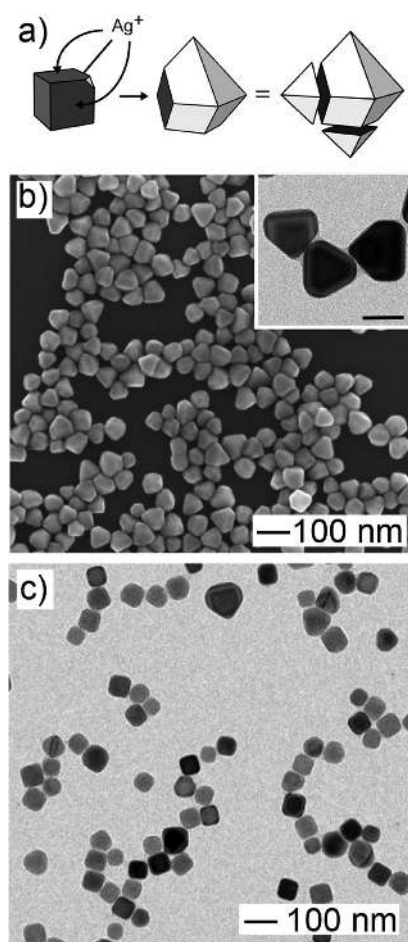
Figure 9. (a) Proposed mechanism for the unsymmetrical growth of a cubic seed. Silver ions reduced more rapidly on three {100} faces adjacent to the truncated corner, leading to the formation of an anisotropically truncated octahedron. For comparison, an octahedron is also shown with three of the corners removed. Note that the third detached corner is not visible at this orientation. White and gray denote {111} and {100} facets, respectively. (b) SEM and (c) TEM images of Ag nanostructures obtained (b) without and (c) with the argon protection. Reproduced with permission from ref 45. Copyright 2009 Wiley−VCH.

size of the final products. For instance, we have demonstrated the synthesis of Pd nanocubes with different edge lengths using the same concentration of Pd precursor, but at different concentrations of $FeCl_3$.[46] In particular, we observed a direct proportional relation, with the increase in size of final products being scaled with the increase in $FeCl_3$ concentration. This strategy has also found use in the preparation of Ag nanocrystals. Similar to the effects of $FeCl_3$, oxidative etching was enhanced when more HCl was present during the nucleation stage, leading to reduction in number of seeds and an increase in size for the resultant nanocrystals. For example, the edge length of Ag nanocubes was tuned from 54 to 86 and 126 nm when the HCl concentration was increased from 0.21 to 0.28, and 0.35 mM, respectively.[47]

5.4. Control of Morphology. *5.4.1. Truncation of Sharp Features.* Generally, oxidative etching of a nanocrystals tend to start from sites with sharp features on the surface.[48] These sites, such as corners, are rich in low-coordination atoms. Removal of atoms from these sites reduces the total surface energy of the nanocrystal, making the final structure more thermodynami-

cally favored.[49,50] For example, Ag nanocubes were found to be gradually truncated and ultimately transformed into spheres after being aged with $Fe(NO_3)_3$ solution. The diameters of the spheres were found to be roughly the same as the edge lengths of the original cubes. To this end, this strategy is considered to be an effective route to the preparation of Ag nanospheres with controlled sizes and in high quality. Similar to nanocubes, the sharp corners of triangular silver nanoplates were also found to be sensitive to oxidative etching. Their corners were increasingly rounded when they were placed in a heated (80 °C) water bath for different periods of time. The rounding process caused shifts to the LSPR peaks of the nanoplate solution, resulting in changes in color. This phenomenon makes this system potentially useful as an indicator of environmental changes. In addition, this kind of etching was also observed for Au nanocrystals with a one-dimensional nanostructure, such as rods and bipyramids. For example, when an aqueous suspension of Au nanorods was bubbled with O_2 in HCl solutions at an elevated temperature, or mixed with an etchant containing Fe^{3+}, persulfate ($S_2O_8^{2-}$), cyanide (CN^-), or hydrogen peroxide (H_2O_2), significant truncation occurred and the nanocrystals were transformed into ricelike or spherical nanoparticles.[51−55] The decrease in intensity, along with the blue-shift, of the longitudinal SPR peak of Au nanorods as a function of the oxidation time, coupled with the corresponding TEM images, confirmed the process of oxidative etching and shape evolution.

5.4.2. Facet Selectivity. Typically, polyhedral noble-metal nanocrystals are enclosed by various types of facets. Owing to different density of atomic steps, ledges, and kinks, these facets can have different surface energies. In general, the surface energy of the three typical low-index facets of an fcc metal follows the trend of $\gamma(111) < \gamma(100) < \gamma(110)$. In this regard, oxidative etching is expected to exhibit specific selectivity toward different facets owing to the difference in surface energy. This principle was demonstrated in a recent study by etching single-crystal Ag nanoparticles using a mixture of NH_4OH and H_2O_2.[56] Single-crystal Ag nanoparticles were chosen as the etching targets due to the fact that these nanocrystals are free of defects, thus excluding the possible influence of defect sites on the selectivity. It was found that the etching rate on the {111} facets of Ag nanocrystals was much higher than that on the {100} facets. Owing to the anisotropy in etching, the morphology of resultant Ag nanocrystals was observed to successively transform from octahedrons into concave octahedrons, eventually yielding octapods as the concentration of etchant was increased (Figure 10a−d). To illustrate this phenomena quantitatively, we evaluated the etching rates on two types of facets by measuring the average thickness of the resulting nanocrystals in both directions. As shown panels in e and f in Figure 10, the etching of {100} facets proceeded rapidly with the addition of more etchant solution, whereas very little etching occurred on the {111} facets. This facet selectivity can also be observed when the etchant was applied to Ag cuboctahedral nanocrystals enclosed by both {100} and {111} facets. Similarly, lower etchant concentrations result in exposed triangular {111} facets and recessed square {100} facets, whereas higher concentrations led to the formation of octapod nanocrystals.

5.4.3. Fabrication of Hollow Metal Nanostructures. Compared to their solid counterparts, hollow metal nanostructures often exhibit exceptional optical, electronic, and catalytic properties due to the increased surface area, reduced density,
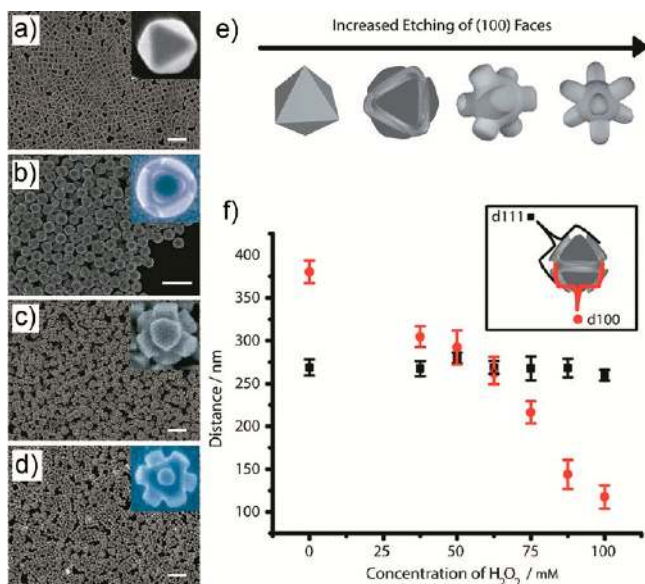
Figure 10. (a−d) SEM images following the etching progress of Ag octahedral nanocrystals. These were obtained by mixing Ag octahedra with increased concentration of etching solution. The scale bars are 1 μm. (e) Schematic showing the progressive etching of the {100} faces of Ag octahedra. (f) Plot showing the effect of etching on the thickness of {100} and {111} faces as a function of etching concentration, demonstrating the selective nature of the 9:1 NH_4OH/H_2O_2 etching solution. Reproduced with permission from ref 56. Copyright 2009 American Chemical Society.

Figure 11. TEM images of the Pd nanostructures at different reaction stages of one batch synthesis: (a) t = 18 h; (b) t = 20 h; (c) t = 21 h; (d) t = 22 h; (e) t = 24 h; and (f) t = 28 h. The upper right and lower left insets show enlarged TEM and SEM images of an individual particle taken from each product, respectively. Reproduced with permission from ref 59. Copyright 2005 Wiley−VCH.

and broadly tunable LSPR.[57] Using oxidative etching, the interior of a solid nanocrystal can be readily removed, making it a facile method for creating hollow nanostructures.[58] For example, single-crystal Pd nanoboxes and nanocages could be obtained during the synthesis of Pd nanocubes in air at an elevated temperature.[59] The reaction can be divided into six distinctive stages based on microscopic and spectroscopic observations. Reduction of $[PdCl_4]^{2-}$ to Pd atoms dominated until t = 18 h (Figure 11a), with the Pd atoms nucleating and growing into nanocubes possessing slightly truncated corners. Oxidative etching of the Pd nanocubes by O_2 began to surpass the reduction process at t = 20 h. Small pits were observed in the surfaces of individual Pd nanocubes (Figure 11b), implying that the corrosion was initiated locally rather than uniformly over the entire surface of each cube. In the next one hour, the interior of each cube became increasingly empty while the size of the hole in the surface started to shrink, forming a box with relatively thick walls (Figure 11c). After another one hour, the inner void further increased in size and each Pd cube evolved into a completely empty box with truncated corners (Figure 11d). Note that the hole in the surface had by now disappeared so that the nanobox was enclosed by smooth walls with a thickness of about 8 nm. Small holes appeared at the corners of each nanobox if the reaction was continued beyond this point. Holes of about 10 nm in diameter punctured each corner at t = 24 h (Figure 11e), thus turning the nanobox into a nanocage. The Pd nanocage had an edge length of approximately 48 nm and was characterized by a uniform wall thickness of about 6 nm. The nanocage finally evolved into a ring (probably through additional etching and Ostwald ripening), thus causing the wall thickness to increase from 6 to 10−20 nm (Figure 11f). This strategy can also be extended to remove one of the metals from binary nanocrystals in order to obtain monometallic nanocryst-
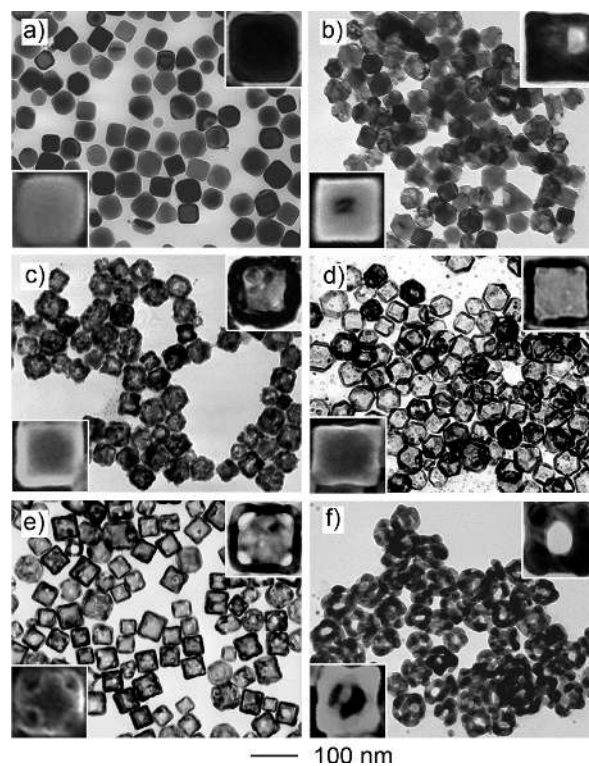
als with hollow interiors. For example, Au cubic nanocages and nanoframes could be obtained via the selective removal of Ag from Au−Ag nanoboxes with an aqueous etchant containing $Fe(NO_3)_3$, NH_4OH, or H_2O_2.[60,61] Additionally, the Pd cores of Pd−Rh core−frame concave nanocubes could be selectively removed by reacting with Fe^{3+} species, producing Rh cubic nanoframes with a unique open structure.[62]

5.4.4. Galvanic Replacement. When metallic ions, like Au^{3+} or Au^+, are employed as the oxidative etchant, it is possible to generate zerovalent species during the oxidation of preformed nanocrystals such as Ag nanocubes. In this case, the oxidization of Ag proceeds simultaneously with the reduction of Au^{3+} or Au^+ ions, leading to the formation of nanostructures composed of Au−Ag alloys. This process is also known as galvanic replacement. It provides a simple and effective method for the preparation of alloyed and, in most cases, hollow/porous nanostructures when metal nanocrystals made of Ag, Pd, or Cu are used as sacrificial templates.[63−67] The driving force for the galvanic replacement reaction can be ascribed to the electrical potential difference between the two metals, with one metal acting as the cathode and the other metal as the anode. For the Au/Ag system the standard reduction potential of $AuCl_4^-$/Au pair (0.99 V vs SHE) is higher than that of Ag^+/Ag pair (0.80 V vs SHE), causing Ag nanostructures to be oxidized by $AuCl_4^-$ according to the following reaction

$$3Ag(s) + AuCl_4^-(aq) = Au(s) + 3Ag^+(aq) + 4Cl^-(aq)$$
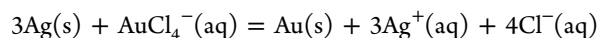
The electrons generated in the oxidation process migrate to the surface of the Ag nanocrystals, where they reduce $AuCl_4^-$ to Au atoms. Because Au and Ag solids share the same fcc structure,

with closely matched lattice constants (4.0786 and 4.0862 Å, respectively), the Au atoms are able to epitaxially nucleate and grow into a shell on the surface of the Ag template. The thickness of the shell is determined by reaction stoichiometry and the amount of HAAuCl4 added into the reaction solution.

Figure 12a summarizes all major steps involved in the formation of Au−Ag nanocages with well-controlled pores at
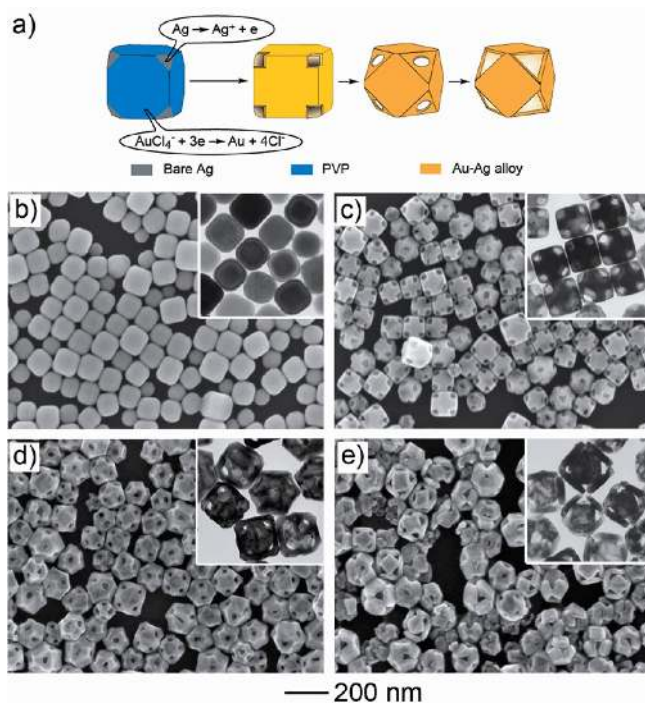

Figure 12. (a) Schematic illustration detailing all major steps involved in the formation of Au−Ag nanocages with well-controlled pores at the corners. The success of this synthesis relies on the use of Ag nanocubes bearing truncated corners with {111} facets to react with aqueous HAuCl$_4$. The pore size is mainly determined by the molar ratio of HAuCl$_4$ to Ag. (b-e) SEM images of Ag nanocubes with truncated corners titrated with 0.1 mM HAuCl$_4$ with the volume of (b) 0, (c) 0.6, (d) 1.6, and (e) 3.0 mL, respectively. The insets show TEM image of each corresponding sample. Reproduced with permission from ref 68. Copyright 2006 American Chemical Society.

the corners by employing Ag nanocubes with truncated corners as the templates.[68] Because poly(vinyl pyrrolidone) (PVP, a capping agent and stabilizer commonly used in the polyol synthesis of noble-metal nanocrystals) tends to preferentially cover the {100} rather than {111} facets,[69] the corner regions unprotected by PVP will serve as the primary sites for the dissolution of Ag when an aqueous solution of HAuCl$_4$ is introduced. As such, well-defined pores form at all corners of the nanobox. Figure 12, b-e, shows SEM and TEM (insets) images of the nanostructures obtained at different stages of the reaction after the Ag truncated nanocubes had been mixed with aqueous HAuCl$_4$. The reaction started simultaneously from each corner of a truncated nanocube while the Au atoms were mainly deposited on the side faces (Figure 12c). As a result, cubic nanocages with well-defined pores at all corners (Figure 12d) were obtained as one of the intermediate structures. In the course of this reaction, the area ratio of {111} to {100} facets increased as a result of surface reconstruction driven by surface free energy minimization. Because the pores were located on the {111} facets, their sizes were gradually enlarged until the

area of {111} facets could not be increased any more. At this point, the product was bound by {100} facets with triangular pores at each corner (Figure 12e). Finally, by adding more AuCl$_4^-$ solution, dealloying of the nanocages would continue, leading to their fragmentation into small pieces.[70,71]

The morphology of the template can also influence the path of the galvanic replacement reaction. For example, when an aqueous solution of HAuCl$_4$ was mixed with Pd nanorods, the resultant Au atoms did not coat the entire surface of the Pd nanorods to generate either a core−sheath or a hollow structure.[72] Instead, the nucleation and deposition of Au was localized to the ends of a Pd nanorod, leading to the formation of a Pd−Au tadpole. No such phase segregation was observed when isotropic Pd nanocrystals (i.e., nanocubes) were employed as the sacrificial templates instead of nanorods. It is believed that in the early stages of the reaction, Au is deposited onto both ends of the rods because repulsive forces tend to push the electrons there. At a later stage, a transition from two-end to one-end growth occurred as a result of Ostwald ripening, leading to the formation of a Pd−Au tadpole composed of a Au head and a Pd tail.

Galvanic replacement was also found to be highly dependent on the reaction stoichiometry. For example, a change of stoichiometry between Au deposition and Ag oxidation in a reaction can lead to differences in the morphology, composition, and optical properties of the products.[73] According to the stoichiometry between Ag and AuCl$_4^-$, only one Au atom is formed for every three Ag atoms being oxidized. If AuCl$_4^-$ is replaced by AuCl$_2^-$, each Ag atom being oxidized will generate one Au atom. Because the standard reduction potential of the AuCl$_2^-$/Au pair (1.11 V vs SHE) is also higher than that of Ag$^+$/Ag pair, Ag nanocubes can still be oxidized by AuCl$_2^-$. The change to the amount of Ag consumed relative to the amount of Au generated during the reaction impacts the alloying and dealloying processes. For example, in later stages of replacement, AuCl$_4^-$ dealloyed Ag from the walls of the Au−Ag alloy nanoboxes, thus forming porous nanocages. In contrast, the reaction with AuCl$_2^-$ produced nanoframes. It should be noted that AuCl$_2^-$ did not completely dealloy Ag from the Au−Ag product even when excess AuCl$_2^-$ solution was added.[74]

In addition to reaction with Ag and other metals, Au^{3+} salt precursors could also serve as an effective etchant for Au itself. Typically, when Au^{3+} ions were mixed with Au nanocrystals, the Au atoms on the surface would react with the Au^{3+} ions to form Au$^+$ ions. Because Au$^+$ ions were unstable, they disproportionated into Au atoms and Au^{3+} ions again. After the newly formed Au atoms had been deposited back onto the original nanocrystals, the overall shape could be altered. For example, polyhedral Au nanocrystals transformed into spherical Au nanocrystals by aging with HAuCl$_4$ solution.[75] The shape evolution process could be completed within a time frame ranging from a few minutes to several days, depending on the particle size. This work clearly showed that the rates for etching and regrowth could be easily controlled by simply varying the concentration of HCl, which promoted the formation of product with different sizes.

5.4.5. Etching and Regrowth. The presence of a suitable reductant in an etching system may introduce a possible pathway for surface regrowth. The reduction of the ions generated from the dissolution of the original nanocrystals and redeposition of the newly formed atoms play an important role in determining the size and shape of the final product. For

example, we recently observed an interesting ripening process for Pd nanocrystals, as caused by a combined action of oxidative etching and subsequent regrowth (Figure 13a).[76] Significantly,
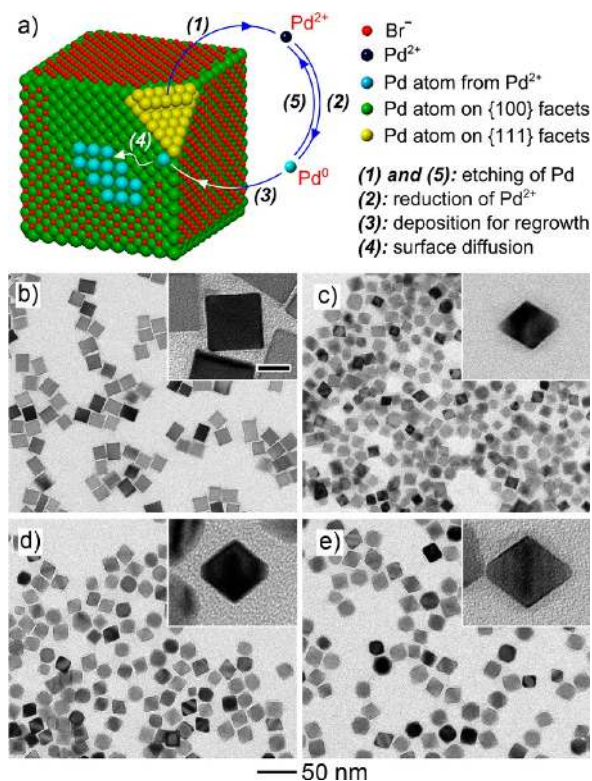

Figure 13. (a) Schematic illustration of the five major steps involved in the oxidative etching and regrowth process. Because all the side faces of the Pd cube were capped by Br$^-$ ions, Pd atoms were mainly etched from the corner(s), and the resultant Pd^{2+} ions were subsequently reduced and deposited onto the side faces. (b−e) TEM images of (b) Pd cubes of 18 nm in edge length and (c−e) Pd octahedrons of 13, 18, and 23 nm in edge length, which were prepared by etching with the addition of (c) 180, (d) 120, and (e) 60 μmol HCl, respectively. The scale bar in the inset of b is 10 nm and applies to all other insets. The scale bar of 50 nm applies to b−e. Reproduced with permission from ref 76. Copyright 2013 American Chemical Society.

Pd nanocubes of one size could be transformed into octahedrons with a range of different but controllable sizes depending on the concentration of the etchant (Figure 13, b−e). In a typical procedure, triethylene glycol (Tri-EG) and HCl/O$_2$ pair served as the reductant and oxidative etchant, respectively. Five major steps were involved in the transformation process. Owning to the passivation of all side faces of a Pd nanocube by Br$^-$ ions and the high energy associated with corner sites, oxidative etching and removal of Pd atoms started from the corners and along the ⟨111⟩ direction (step 1). The Pd^{2+} ions released from the etching were then reduced back to zerovalent atoms (step 2) by Tri-EG. These atoms were deposited onto the edges of the nanocubes, due to the high energy of these sites and the unavailability of corner sites (step 3). The migration of these atoms from edges to adjacent side faces subsequently occurred *via* surface diffusion (step 4). Combined together, these steps resulted in the gradual transformation of the Pd nanocubes into octahedrons. It should be noted that the newly generated Pd atoms could be oxidized back into the ionic form in a strongly corrosive environment (step 5). As such, it was possible to tune the sizes

of the resultant octahedrons by manipulating the rate of oxidative etching relative to the rate of regrowth. In this case, the etching rate was controlled by simply adjusting the concentration of HCl. At high concentrations of HCl, the Pd atoms, derived from the reduction of Pd^{2+} cations, were quickly oxidized into ions. Thus, steps 3 and 4 were suppressed because of the significant acceleration of step 5. As such, regrowth on the particle surface became negligible relative to the etching process, resulting in the formation of Pd octahedrons with relatively small sizes. Conversely, if the concentration of HCl was relatively low, a large fraction of atoms etched from the corners would be reduced and redeposited back onto the nanocube. In this case, the total volume of the final octahedron would be essentially the same as that of the initial nanocube.

6. CONCLUDING REMARKS

As a common phenomenon in our daily life, oxidative etching has been demonstrated to play an important role in the synthesis of metal nanocrystals. Significant progress has been made in this field in recent years, and we are now able to offer examples of oxidative etching observed in both hydrophilic and hydrophobic systems. This process can be monitored and analyzed using techniques such as electron microscopy, UV−vis spectroscopy, and inductively coupled plasma mass spectrometry (ICP-MS). When needed, oxidative etching can also be eliminated via several approaches, leading to the synthesis of various types of twinned nanocrystals with reasonable yields. We also demonstrated a range of interesting applications, including the use of oxidative etching to control the crystallinity, growth, size, and morphology of noble-metal nanocrystals.

Although considerable progress has been made in this research area, we believe the following aspects still need to be addressed in further studies: (i) Development of advanced tools for in situ monitoring of the etching process. Although ex situ UV−vis and ICP-MS analyses, as well as TEM imaging, have provided a wealth of information about the oxidative etching process, some of the details about the changes in nanoparticle shape and crystallinity could be missed between those points of analysis. Advanced microscopy techniques (e.g., liquid cell TEM) and in situ synchrotron X-ray techniques (e.g., in situ synchrotron X-ray transmission microscopy and high-energy synchrotron X-ray diffraction, among others) may be of great help in visualizing and monitoring the oxidative etching process in situ.[77−81] In addition, (ii) Establishment of a general index to quantitatively describe and thus compare oxidative etching strength. Different etchants may all be effective for oxidative etching of a specific material, but it is difficult to compare the relative etching strength of these species. This can be further complicated by the variation in etchant concentration or ligand type present in the system. To this end, it would be of great advantage to establish a general index of etching strength, allowing people to rationally and efficiently engineer an oxidative etchant for a specific application. In short, the challenge now is to continuously elucidate the oxidative mechanism and to achieve a better control of oxidative etching, turning it into a powerful and versatile tool for manipulating nucleation, growth, and shape transformation of metal nanocrystals.[82]

■ AUTHOR INFORMATION

Corresponding Author
*E-mail: younan.xia@bme.gatech.edu.

Notes

The authors declare no competing financial interest.

■ ACKNOWLEDGMENTS

■ REFERENCES

(1) Bradford, S. A. *Corrosion Control*, second ed.; CASTI Publishing: Edmonton, Canada, 2001.

(2) Moon, C.-Y.; Kim, Y.-S.; Lee, E.-C.; Jin, Y.-G.; Chang, K. J. *Phys. Rev. B* **2002**, *65*, 155401.

(3) de Theije, F. K.; Roy, O.; van der Laag, N. J.; van Enckevort, W. J. P. *Diam. Relat. Mater.* **2000**, *9*, 929.

(4) Lee, S. M.; Lee, Y. H.; Hwang, Y. G.; Hahn, J. R.; Kang, H. *Phys. Rev. Lett.* **1999**, *82*, 217.

(5) Sui, Y.; Fu, W.; Zeng, Y.; Yang, H.; Zhang, Y.; Chen, H.; Li, Y.; Li, M.; Zou, G. *Angew. Chem., Int. Ed.* **2010**, *49*, 4282.

(6) Yoshimoto, M.; Yoshida, K.; Maruta, H.; Hishitani, Y.; Koinuma, H.; Nishio, S.; Kakihana, M.; Tachibana, T. *Nature* **1999**, *399*, 340.

(7) Xia, Y.; Xiong, Y.; Lim, B.; Skrabalak, S. E. *Angew. Chem., Int. Ed.* **2009**, *48*, 60.

(8) Thürmer, K.; Williams, E.; Reutt-Robey, J. *Science* **2002**, *297*, 2033.

(9) Wiley, B.; Herricks, T.; Sun, Y.; Xia, Y. *Nano Lett.* **2004**, *4*, 1733.

(10) Im, S. H.; Lee, Y. T.; Wiley, B.; Xia, Y. *Angew. Chem., Int. Ed.* **2005**, *44*, 2154.

(11) Wang, Y.; Zheng, Y.; Huang, C. Z.; Xia, Y. *J. Am. Chem. Soc.* **2013**, *135*, 1941.

(12) Zhang, Q.; Li, W.; Moran, C.; Zeng, J.; Chen, J.; Wen, L.-P.; Xia, Y. *J. Am. Chem. Soc.* **2010**, *132*, 11372.

(13) Rycenga, M.; Cobley, C. M.; Zeng, J.; Li, W.; Moran, C. H.; Zhang, Q.; Qin, D.; Xia, Y. *Chem. Rev.* **2011**, *111*, 3669.

(14) Wang, Y.; Xie, S.; Liu, J.; Park, J.; Huang, C. Z.; Xia, Y. *Nano Lett.* **2013**, *13*, 2276.

(15) Xiong, Y.; Chen, J.; Wiley, B.; Xia, Y.; Aloni, S.; Yin, Y. *J. Am. Chem. Soc.* **2005**, *127*, 7332.

(16) Ma, Y.; Li, W.; Zeng, J.; McKiernan, M.; Xie, Z.; Xia, Y. *J. Mater. Chem.* **2010**, *20*, 3586.

(17) Li, Z.; Tao, J.; Lu, X.; Zhu, Y.; Xia, Y. *Nano Lett.* **2008**, *8*, 3052.

(18) Kisner, A.; Heggen, M.; Fernández, E.; Lenk, S.; Mayer, D.; Simon, U.; Offenhäusser, A.; Mourzina, Y. *Chem.—Eur. J.* **2011**, *17*, 9503.

(19) Taguchi, A.; Fujii, S.; Ichimura, T.; Verma, P.; Inouye, Y.; Kawata, S. *Chem. Phys. Lett.* **2008**, *462*, 92.

(20) Teng, X.; Han, W.-Q.; Ku, W.; Hücker, M. *Angew. Chem., Int. Ed.* **2008**, *47*, 2055.

(21) Alam, M. J.; Tsuji, M.; Matsunaga, M. *Bull. Chem. Soc. Jpn.* **2010**, *83*, 92.

(22) Wiley, B.; Sun, Y.; Xia, Y. *Langmuir* **2005**, *21*, 8077.

(23) Korte, K. E.; Skrabalak, S. E.; Xia, Y. *J. Mater. Chem.* **2008**, *18*, 437.

(24) Tsuji, M.; Miyamae, N.; Hashimoto, M.; Nishio, M.; Hikino, S.; Ishigami, N.; Tanaka, I. *Colloids Surf., A* **2007**, *302*, 587.

(25) Tsuji, M.; Miyamae, N.; Nishio, M.; Hikino, S.; Ishigami, N. *Bull. Chem. Soc. Jpn.* **2007**, *80*, 2024.

(26) Niu, W.; Li, Z.-Y.; Shi, L.; Liu, X.; Li, H.; Han, S.; Chen, J.; Xu, G. *Cryst. Growth Des.* **2008**, *8*, 4440.

(27) Wang, F.; Li, C.; Sun, L.-D.; Xu, C.-H.; Wang, J.; Yu, J. C.; Yan, C.-H. *Angew. Chem., Int. Ed.* **2012**, *51*, 4872.

(28) Soejima, T.; Kimizuka, N. *J. Am. Chem. Soc.* **2009**, *131*, 14407.

(29) Cheng, Y.; Qiu, C.; Ma, H.; Zhang, X.; Gu, X. *Nanoscale* **2010**, *2*, 685.

(30) Zettsu, N.; McLellan, J. M.; Wiley, B.; Yin, Y.; Li, Z.-Y.; Xia, Y. *Angew. Chem., Int. Ed.* **2006**, *45*, 1288.

(31) Biacchi, A. J.; Schaak, R. E. *ACS Nano* **2011**, *5*, 8089.

(32) Zhang, H.; Xia, X.; Li, W.; Zeng, J.; Dai, Y.; Yang, D.; Xia, Y. *Angew. Chem., Int. Ed.* **2010**, *49*, 5296.

(33) Xiong, Y.; McLellan, J. M.; Yin, Y.; Xia, Y. *Angew. Chem., Int. Ed.* **2007**, *46*, 790.

(34) Lim, B.; Xiong, Y.; Xia, Y. *Angew. Chem., Int. Ed.* **2007**, *46*, 9279.

(35) Wiley, B. J.; Xiong, Y.; Li, Z.-Y.; Yin, Y.; Xia, Y. *Nano Lett.* **2006**, *6*, 765.

(36) Wiley, B. J.; Chen, Y.; McLellan, J. M.; Xiong, Y.; Li, Z.-Y.; Ginger, D.; Xia, Y. *Nano Lett.* **2007**, *7*, 1032.

(37) Zhang, Q.; Moran, C. H.; Xia, X.; Rycenga, M.; Li, N.; Xia, Y. *Langmuir* **2012**, *28*, 9047.

(38) Zeng, J.; Zhu, C.; Tao, J.; Jin, M.; Zhang, H.; Li, Z.-Y.; Zhu, Y.; Xia, Y. *Angew. Chem., Int. Ed.* **2012**, *51*, 2354.

(39) Zhu, C.; Zeng, J.; Tao, J.; Johnson, M. C.; Schmidt-Krey, I.; Blubaugh, L.; Zhu, Y.; Gu, Z.; Xia, Y. *J. Am. Chem. Soc.* **2012**, *134*, 15822.

(40) Xia, X.; Xia, Y. *Nano Lett.* **2012**, *12*, 6038.

(41) Chen, J.; Herricks, T.; Geissler, M.; Xia, Y. *J. Am. Chem. Soc.* **2004**, *126*, 10854.

(42) Chen, J.; Herricks, T.; Xia, Y. *Angew. Chem., Int. Ed.* **2005**, *44*, 2589.

(43) Lim, B.; Lu, X.; Jiang, M.; Camargo, P. H. C.; Cho, E. C.; Lee, E. P.; Xia, Y. *Nano Lett.* **2008**, *8*, 4043.

(44) Xiong, Y.; Cai, H.; Wiley, B. J.; Wang, J.; Kim, M. J.; Xia, Y. *J. Am. Chem. Soc.* **2007**, *129*, 3665.

(45) Cobley, C. M.; Rycenga, M.; Zhou, F.; Li, Z. −Y.; Xia, Y. *Angew. Chem., Int. Ed.* **2009**, *48*, 4824.

(46) Xiong, Y.; Chen, J.; Wiley, B.; Xia, Y.; Yin, Y.; Li, Z.-Y. *Nano Lett.* **2005**, *5*, 1237.

(47) Li, B.; Long, R.; Zhong, X.; Bai, Y.; Zhu, Z.; Zhang, X.; Zhi, M.; He, J.; Wang, C.; Li, Z.-Y.; Xiong, Y. *Small* **2012**, *8*, 1710.

(48) Xiong, Y. *Chem. Commun.* **2011**, *47*, 1580.

(49) Xu, J.; Li, S.; Weng, J.; Wang, X.; Zhou, Z.; Yang, K.; Liu, M.; Chen, X.; Cui, Q.; Cao, M.; Zhang, Q. *Adv. Funct. Mater.* **2008**, *18*, 277.

(50) Zeng, J.; Roberts, S.; Xia, Y. *Chem.—Eur. J.* **2010**, *16*, 12559.

(51) Zou, R.; Guo, X.; Yang, J.; Li, D.; Peng, F.; Zhang, L.; Wang, H.; Yu, H. *CrystEngComm* **2009**, *11*, 2797.

(52) Tsung, C.-K.; Kou, X.; Shi, Q.; Zhang, J.; Yeung, M. H.; Wang, J.; Stucky, G. D. *J. Am. Chem. Soc.* **2006**, *128*, 5352.

(53) Jana, N. R.; Gearheart, L.; Obare, S. O.; Murphy, C. J. *Langmuir* **2002**, *18*, 922.

(54) Kou, X.; Ni, W.; Tsung, C.-K.; Chan, K.; Lin, H.-Q.; Stucky, G. D.; Wang, J. *Small* **2007**, *3*, 2103.

(55) Chandrasekar, G.; Mougin, K.; Haidara, H.; Vidal, L.; Gnecco, E. *Appl. Surf. Sci.* **2011**, *257*, 4175.

(56) Mulvihill, M. J.; Ling, X. Y.; Henzie, J.; Yang, P. *J. Am. Chem. Soc.* **2009**, *132*, 268.

(57) Skrabalak, S. E.; Chen, J.; Sun, Y.; Lu, X.; Au, L.; Cobley, C. M.; Xia, Y. *Acc. Chem. Res.* **2008**, *41*, 1587.

(58) Huang, C.-C.; Hwu, J. R.; Su, W.-C.; Shieh, D.-B.; Tzeng, Y.; Yeh, C.-S. *Chem.—Eur. J.* **2006**, *12*, 3805.

(59) Xiong, Y.; Wiley, B.; Chen, J.; Li, Z.-Y.; Yin, Y.; Xia, Y. *Angew. Chem., Int. Ed.* **2005**, *44*, 7913.

(60) Lu, X.; Au, L.; McLellan, J.; Li, Z.-Y.; Marquez, M.; Xia, Y. *Nano Lett.* **2007**, *7*, 1764.

(61) Zhang, Q.; Cobley, C. M.; Zeng, J.; Wen, L.-P.; Chen, J.; Xia, Y. *J. Phys. Chem. C* **2010**, *114*, 6396.

(62) Xie, S.; Lu, N.; Xie, Z.; Wang, J.; Kim, M. J.; Xia, Y. *Angew. Chem., Int. Ed.* **2012**, *51*, 10266.

(63) Chen, J.; Wiley, B.; McLellan, J.; Xiong, Y.; Li, Z.-Y.; Xia, Y. *Nano Lett.* **2005**, *5*, 2058.

(64) Xie, S.; Jin, M.; Tao, J.; Wang, Y.; Xie, Z.; Zhu, Y.; Xia, Y. *Chem.—Eur. J.* **2012**, *18*, 14974.

(65) Zhang, H.; Jin, M.; Liu, H.; Wang, J.; Kim, M. J.; Yang, D.; Xie, Z.; Liu, J.; Xia, Y. *ACS Nano* **2011**, *5*, 8212.

(66) Liu, M.; Zheng, Y.; Xie, S.; Li, N.; Lu, N.; Wang, J.; Kim, M. J.; Guo, L.; Xia, Y. *Phys. Chem. Chem. Phys.* **2013**, *15*, 11822.

(67) McEachran, M.; Keogh, D.; Pietrobon, B.; Cathcart, N.; Gourevich, I.; Coombs, N.; Kitaev, V. *J. Am. Chem. Soc.* **2011**, *133*, 8066.

(68) Chen, J.; McLellan, J. M.; Siekkinen, A.; Xiong, Y.; Li, Z.-Y.; Xia, Y. *J. Am. Chem. Soc.* **2006**, *128*, 14776.

(69) Zeng, J.; Zheng, Y.; Rycenga, M.; Tao, J.; Li, Z.-Y.; Zhang, Q.; Zhu, Y.; Xia, Y. *J. Am. Chem. Soc.* **2010**, *132*, 8552.

(70) Sun, Y.; Xia, Y. *Nano Lett.* **2003**, *3*, 1569.

(71) Cobley, C. M.; Zhang, Q.; Song, W.; Xia, Y. *Chem. Asian J.* **2011**, *6*, 1479.

(72) Camargo, P. H. C.; Xiong, Y.; Ji, L.; Zuo, J. M.; Xia, Y. *J. Am. Chem. Soc.* **2007**, *129*, 15452.

(73) Au, L.; Lu, X.; Xia, Y. *Adv. Mater.* **2008**, *20*, 2517.

(74) Lu, X.; Chen, J.; Skrabalak, S. E.; Xia, Y. *Proc. Inst. Mech. Eng., Part N* **2007**, *221*, 1.

(75) Rodríguez-Fernández, J.; Pérez-Juste, J.; Mulvaney, P.; Liz-Marzán, L. M. *J. Phys. Chem. B* **2005**, *109*, 14257.

(76) Liu, M.; Zheng, Y.; Zhang, L.; Guo, L.; Xia, Y. *J. Am. Chem. Soc.* **2013**, DOI: 10.1021/ja406344j.

(77) Liu, Y.; Lin, X.-M.; Sun, Y.; Rajh, T. *J. Am. Chem. Soc.* **2013**, *135*, 3764.

(78) Liao, H.-G.; Zheng, H. *J. Am. Chem. Soc.* **2013**, *135*, 5038.

(79) Jungjohann, K. L.; Bliznakov, S.; Sutter, P. W.; Stach, E. A.; Sutter, E. A. *Nano Lett.* **2013**, *13*, 2964.

(80) Sun, Y.; Wang, Y. *Nano Lett.* **2011**, *11*, 4386.

(81) Peng, S.; Okasinski, J. S.; Almer, J. D.; Ren, Y.; Wang, L.; Yang, W.; Sun, Y. *J. Phys. Chem. C* **2012**, *116*, 11842.

(82) Macpherson, J. V.; Slevin, C. J.; Unwin, P. R. *J. Chem. Soc., Faraday. Trans.* **1996**, *92*, 3799.

(83) http://www.bushman.cc/corrosion_photos.html. Bushman & Associates: Medina, OH (last accessed May, 2013).